https://doi.org/10.5194/egusphere-2025-368
Preprint. Discussion started: 4 February 2025

Global Patterns and Trends in Ground-Level Ozone Chemical Formation Regimes from 1996 to 2022

Yu Tian[1], Siyi Wang[1], Xiaomeng Jin[1, *]

[1]Department of Environmental Sciences, Rutgers, The State University of New Jersey, New Brunswick, NJ 08901, U.S.A

Correspondence to: Xiaomeng Jin (xiaomeng.jin@rutgers.edu)

Abstract. Ground-level ozone (O_3) formation in urban areas is nonlinearly dependent on the relatively availability of its precursors: oxides of nitrogen (NO_x) and volatile organic compounds (VOCs). To mitigate O_3 pollution, a crucial question is to identify the O_3 formation regime (NO_x-limited or VOC-limited). Here we leverage ground-based O_3 observations alongside space-based observations of O_3 precursors, namely NO_2 and formaldehyde (HCHO), to study the long-term shifts in O_3 chemical regimes across global source regions. We first derive the regime threshold values for satellite-derived HCHO/NO_2 ratio by examining its relationship with the O_3 weekend effect. We find that a regime transition from VOC-limited to NO_x-limited occurs around 3.5 for HCHO/NO_2 with regional variations. By integrating data from four satellite instruments, including GOME, SCIAMACHY, OMI, and TROPOMI, we build a 27-year (1996 - 2022) satellite HCHO/NO_2 record, from which we assess the long-term trends in O_3 production regimes. A discernible global trend towards NO_x-limited regimes is evident, particularly in developed regions such as North America, Europe, and Japan, with emerging trends in developing countries like China and India over the past two decades. This shift is supported by both increasing HCHO/NO_2 ratios and a diminishing O_3 weekend effect. Yet, urban areas still hover in the VOC-limited and transitional regime on the basis of annual averages. Our findings stress the importance of adaptive emission control strategies to mitigate O_3 pollution.

1 Introduction

Ozone (O_3) near the surface is an air pollutant with profound implications for human health and Earth's ecological system (Chiu et al., 2023; Nuvolone et al., 2018; Mills et al., 2016; Felzer et al., 2007). It is known to cause respiratory and cardiovascular diseases (Who, 2013). Chronic exposure to O_3 has been linked to an estimated 1.04 to 1.23 million premature mortalities globally in 2010, primarily due to respiratory ailments (Malley et al., 2017), and this issue of O_3-related deaths has the potential to worsen despite the improvement of other air pollutants like fine particulate matter (Lu et al., 2018; Li et al., 2019; Wang et al., 2021). In addition to its harmful effects on human health, O_3 poses a threat to other species by inducing DNA damage in animals and affecting crop productivity and yield through disrupting the plant microflora (Manisalidis et al., 2020).

Ground-level O_3 is a secondary air pollutant, formed through photochemical reactions between oxides of nitrogen (NO_x) and volatile organic compounds (VOCs). At ground level, O_3 formation is mostly in NO_x-limited regime globally, especially in rural or sparsely populated regions (Monks et al., 2015). In areas with high NO_x emissions and relatively

https://doi.org/10.5194/egusphere-2025-368
Preprint. Discussion started: 4 February 2025

low HCHO emissions, such as urban and metropolitan centers, O_3 formation can become NO_x-saturated, or in other words, VOC-limited. Freshly emitted NO, particularly from vehicular traffic, can locally deplete O_3 by reacting with it (Solberg et al., 2005), thereby curtailing O_3 accumulation in the immediate vicinity. Consequently, lower O_3 concentrations are typically observed in urban areas (Paoletti et al., 2014; Simon et al., 2024). Over the past several decades, the evolution of global O_3 formation has been shaped by a complex interplay of socio-economic factors, including varying industrial activities and population movements, as well as environmental policies and changing climate (Pfister et al., 2014; Zhang et al., 2019). The combined effects of these factors are highly intricate. For instance, sustained declines in NO_x and VOCs emissions have led to reductions in peak O_3 concentrations in many developed countries, but mitigating O_3 exposure at the urban scale is still challenging owing to the nonlinearity of O_3-NO_x-VOC chemistry (Simon et al., 2016). Therefore, understanding the O_3 production regimes transition and its drivers are essential for devising effective mitigation strategies.

O_3 sensitivity cannot be directly observed, which is often diagnosed through analyzing the relationship between observed O_3 and its precursors, or by using measurements of indicator species such as NO_y, formaldehyde (HCHO), reactive nitrogen (NO_y), hydrogen peroxide (H_2O_2), nitric acid (HNO_3) (Tonnesen and Dennis, 2000; Sillman, 1999, 1995). However, ground-based measurements of these indicators are often limited, making satellite remote sensing a vital alternative for expanding the monitoring of these atmospheric species. Satellites provide retrievals of two key species: HCHO (Fu et al., 2007; Palmer et al., 2003), which is nearly proportional to the summed rate of VOC reactions with hydroxyl radicals (OH) and thus serves as an effective VOCs tracer (Sillman, 1995), and nitrogen dioxide (NO_2), which is prevalent in the boundary layer atmosphere and represent the majority of NO_x (Duncan et al., 2010). The ratio of HCHO to NO_2 (HCHO/NO_2) has been used to infer O_3-NO_x-VOC sensitivity (Choi et al., 2012; Jin and Holloway, 2015; Martin et al., 2004; Duncan et al., 2010; Jin et al., 2020; Jin et al., 2017). An important issue to use satellite HCHO/NO_2 is to determine the threshold values separating the NO_x-limited and VOC-limited regimes. Martin et al. (2004) and Duncan et al. (2010) use 1 and 2 regime threshold values, but follow-up studies show that the regime threshold values are uncertain (Jin et al., 2017; Souri et al., 2023; Wang et al., 2021; Schroder et al., 2017).

Over the past two decades, the global distributions of HCHO and NO_2 concentrations have been shaped by diverse emission reduction policies, resulting in distinct regional changes. In terms of NO_2, many anthropogenic regions have witnessed non-linear shifts or reversal years in NO_2 pollutant levels (Georgoulias et al., 2019). In developed regions such as the U.S. and European countries, substantial reductions in NO_x emissions have been achieved, largely due to stringent national regulations (Russell et al., 2012; Krotkov et al., 2016; Toro et al., 2021; Gov.Uk, 2024) , whereas in developing regions, NO_x emission reductions have normally lagged behind. According to Zhao et al. (2013), there was a surge in NO_x emissions in China until around 2010, after which a decline was observed. This decrease has been linked to technological advancements and the implementation of emission control measures in key industries (Sun et al., 2018). Given the diverse trends of O_3 precursor emissions, less is known how the O_3 production regime has changed over the past decades because of the emission changes. Here we aim to identify the long-term trends in satellite HCHO/NO_2 and the reversal years in different region, which could signal a change in the direction of O_3 chemical regime changes.

Another widely used method to characterize O_3 formation regimes is through comparing the weekend versus weekday

https://doi.org/10.5194/egusphere-2025-368
Preprint. Discussion started: 4 February 2025

difference (WE-WD) in O_3 levels and its precursors. Under high NO_x, O_3 production rates paradoxically increase as NO_x concentration fall; conversely, in scenarios with low NO_x, O_3 production rates decline. In most urban areas, characterized by high NO_x levels, O_3 concentrations frequently display a significant rise on weekends relative to weekdays. Reasons for this "O_3 weekend effect" can be multifaceted and region-specific, involving reduced NO_x concentrations altering VOC ratios, timing shifts in NO_x emissions, increased VOCs and NO_x emissions on weekend nights, and enhanced sunlight due to lower particulate matter emissions (Carb, 2003). This distinctive WE-WD O_3 pattern has been observed globally, first documented in New York City, U.S. (Cleveland et al., 1974), and subsequently reported in various regions including Europe (Sicard et al., 2020; Adame et al., 2014), East Asia: Tokyo, Japan (Yasuhiro et al.), the Pearl River Delta (Zou et al., 2019), the North China Plain (Wang et al., 2014), the Yangtze River Delta (Tang et al., 2008) and Taiwan (Tsai, 2005), North America: Mexico (Stephens et al., 2008) and whole U.S (Jaffe et al., 2022; Atkinson-Palombo et al., 2006), as well as major cities in Latin America: Santiago, Chile (Seguel et al., 2012) and Rio de Janeiro, Brazil (Martins et al., 2015). The varying O_3 weekend effect provides an opportunity to evaluate the chemical regimes of O_3 (Simon et al., 2024; Jin et al., 2020).

In this study, we aim to elucidate the long-term shifts in O_3 chemical regimes on a global scale using the two indicators: satellited derived $HCHO/NO_2$ ratios and ground-based observation of O_3 weekend effect. In Section 3.1, we examined the surface WE-WD O_3 concentration as a function of the tropospheric column $HCHO/NO_2$ ratio to identify the thresholds distinguishing different O_3 regimes. In Section 3.2, we analyzed the long-term trend of satellite-based $HCHO/NO_2$ and identified the trend reversals. These two steps set the stage for evaluating the long-term evolution of O_3 production regime. In Section 3.3, we synthesize above analyses with the objective of pinpointing the year when the $HCHO/NO_2$ ratio crossed the critical thresholds, indicating a shift from the VOC-limited to the NO_x-limited regime. The HCHO and NO_2 retrievals integrate 27-year (1996 - 2022) data from four satellite instruments: GOME/ERS-2, SCIAMACHY/ENVISAT, OMI/Aura and TROPOMI/Sentinel-5P. Finally, we assess whether the satellite-based trends in O_3 chemical regimes are consistent with long-term trends of the O_3 weekend effect in Section 3.4. Overall, our goal is to provide a view of O_3 regime changes across regions and decades, which could have implications for environmental policy and air quality management.

2 Data and Methods

2.1 Harmonized Satellite Retrievals of O_3 Precursors

We combine satellite retrievals of tropospheric NO_2 and HCHO vertical columns from four different satellite instruments, including: Global Ozone Monitoring Experiment (GOME), SCanning Imaging Absorption spectroMeter for Atmospheric CHartographY (SCIAMACHY) and Ozone Monitoring Instrument (OMI) and TROPOspheric Monitoring Instrument (TROPOMI). We use satellite-based products developed under the Quality Assurance for Essential Climate Variables (QA4ECV) project, which retrieves NO_2 and HCHO consistently using the same *a priori* profile obtained from TM5-MP (Boersma et al., 2018; Williams et al., 2017; De Smedt et al., 2017; Boersma et al., 2017b, a). The nadir resolution is 320 × 40 km^2 for GOME, 60 × 30 km^2 for SCIAMACHY, 24 × 13 km^2 for OMI and 5.5 × 3.5 km^3

https://doi.org/10.5194/egusphere-2025-368
Preprint. Discussion started: 4 February 2025

for TROPOMI. The overpass time is around 10:00 AM local time for SCIAMACHY and GOME, ~ 1:30 PM for OMI and TROPOMI,

To build the relationship between observed O_3 weekend effect and satellite HCHO/NO_2, we mainly use OMI retrievals of HCHO and NO_2, as it provides the longest record with fine resolution suitable for studying the urban O_3 chemistry, and the overpass time of OMI is well suited to detect the O_3 formation sensitivity during the afternoon as the O_3 photochemical production peaks and when the boundary layer is high and the solar zenith angle is small, maximizing the instrument sensitivity to HCHO and NO_2 in the lower troposphere (Jin and Holloway, 2015; Jin et al., 2017). To investigate the long-term changes in HCHO/NO_2, we construct annual average HCHO and NO_2 using tropospheric NO_2 and HCHO VCD data from the GOME (1996-2001), SCIAMACHY (2002-2003) and OMI (2004-2020) and TROPOMI (2020 - 2022) datasets. GOME and SCIAMACHY and TROPOMI data are harmonized with reference to OMI data with a resolution of 0.25˚ × 0.25˚. The retrieval and harmonization scheme are described in Jin et al. (2020).

2.2 Ground-based O_3 observations

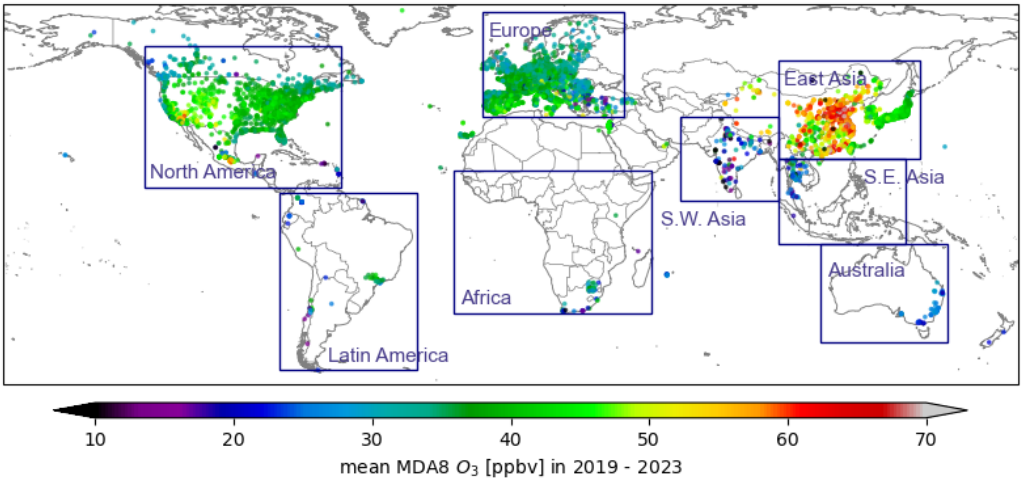

Figure 1: Global distribution of O_3 (unit: ppbv) in the past 5 years (2019-2023). Data are sourced from the TOAR database.

For O_3 data, we rely on TOAR-II database (https://toar-data.org/surface-data, last access: April 2024). Initiated by the Global Atmospheric Chemistry Project (GACP), TOAR has developed a cutting-edge database that provides hourly surface O_3 concentrations on a global scale since 1970 (Schultz et al., 2017), serving as an unparalleled resources for examining temporal trends in surface O_3 levels (Sicard et al., 2020). Notably, the observation records period various across monitoring stations, with earlier data in the U.S., Europe and Japan dating back to the 1970s-1980s, and later in countries like the South Korea and Latin America, starting from 1995 to 2005. For China, South Africa, Southwest Asia, and densely populated Australian areas, records typically begin around 2015. To ensure rigorous study standards, we selected over 8700 stations with at least 5 consecutive years of data for our global analysis. Figure 1 illustrates the distribution of TOAR sites and main regions we focus on.

https://doi.org/10.5194/egusphere-2025-368
Preprint. Discussion started: 4 February 2025

2.3 Building Connections Between Satellite HCHO/NO_2 and Ground-Based WE-WD O_3 Observation

We utilize monthly HCHO/NO_2 derived from the OMI to establish correlations with ground-based TOAR O_3 observation. We extract gridded daily OMI HCHO and NO_2 data (0.25° × 0.25°) for days and grid cells with corresponding O_3 monitoring data, ensuring that both datasets are paired consistently in time and location. To quantify O_3 differences between weekends and weekdays, we designate Sunday to represent weekends and Tuesday to Thursday to represent weekdays, excluding other days to minimize carryover effects from typical workdays and rest-days. For each site and weekly interval throughout the observation period, we calculated the mean differences in MDA8 O_3 concentrations (WE-WD O_3). Given the global scope of this analysis and the inherent complexity in defining distinct O_3 seasons across various regions, we utilize all-year data without seasonal selection. Using t-test at each site or grid to ascertain the statistical significance of WE-WD difference (p-value<0.05). For annual trends, we apply the non-parametric Mann-Kendall test (Kendall, 1975; Mann., 1945) coupled with Theil-Sen's slope estimator (Raj and Koerts, 1992; Sen, 1968). We examine the annual trends in the WE-WD O_3 over 5-year rolling intervals to mitigate the effects of interannual meteorological variability (Pierce et al., 2010).

2.4 Detection of Long-term Trend Reversal in Annual HCHO/NO_2

As most regions show bi-directional trends of O_3 precursors, we hypothesize that a reversal of trend in HCHO/NO_2 can be found during our study period. To identify trend reversal years for the HCHO/NO_2 ratio at each grid point, we adopt the method Georgoulias et al. (2019) used in the analysis of satellite-derived NO_2 trend reversals, originally adapted by Cermak et al. (2010) for studying solar radiation and global brightening trends. The approach is briefly described as follows:

Firstly, for each grid point and for each year *t*, a point score *S*(*t*) is calculated to quantify the potential for a trend reversal:

$$S(t) = \frac{\min(p(B_1),\ p(B_r))}{\mathrm{abs}(B_l - B_r) \times \sigma_{B_{l+r}}} \quad (1)$$

Here, B_1, B_r and B_{1+r} represent the trends calculated over 5-year periods to the left [t - 4, t], right [t, t + 4], and spanning the year [t - 4, t +4], respectively. The 5-year interval is chosen to reduce the impact of interannual meteorology variability. $p(B_1)$ and $p(B_r)$ are the probabilities (p-value) of the trend B being statistically insignificant, while $\sigma_{B_{l+r}}$ signifies the error in trend fitting. The *p*-value of the hypothesis test, with the null hypothesis being a zero slope, using a Wald test with a *t*-distribution.

The time series data for each grid and period are fitted to a linear model:

$$Y_t = A + BX_t + N_t \quad (2)$$

where Y_t is the annual mean value for year *t*, X_t is time variable representing the year, *A* is the annual mean of the first year, *B* is the estimated slope of trend line, and N_t represents the residual, or the discrepancy between the fitted and the

https://doi.org/10.5194/egusphere-2025-368
Preprint. Discussion started: 4 February 2025

observed value.

A year is identified as a trend reversal year if it exhibits the lowest $S(t)$ value, an opposite sign between B_l and B_r ($B_l \times B_r$ <0), and significant trend starts and ends (both $p(B_l)$ and $p(B_r)$ < 0.05). Selecting the year with the lowest $S(t)$ ensures a maximal difference in trends slope (max $|B_l - B_r|$) on either side of the year, with the fitting error of the trend at this juncture, σ_B, being as pronounced as possible. This method is estimated to be capable of identifying reversal years with a very limited error of 0.5-1% and standard deviation between 2 and 5% (Cermak et al., 2010). The trend calculation, based on data spanning 5 years before and after each year, helps to mitigate the impact of short-term extremes in pollutant concentrations, such as the dramatic decrease in emissions during the 2020 COVID-19 pandemic. This approach allows us to identify regions with long-term changes in trends.

3 Results and Discussions

3.1 Identification of regime thresholds for satellite HCHO/NO₂

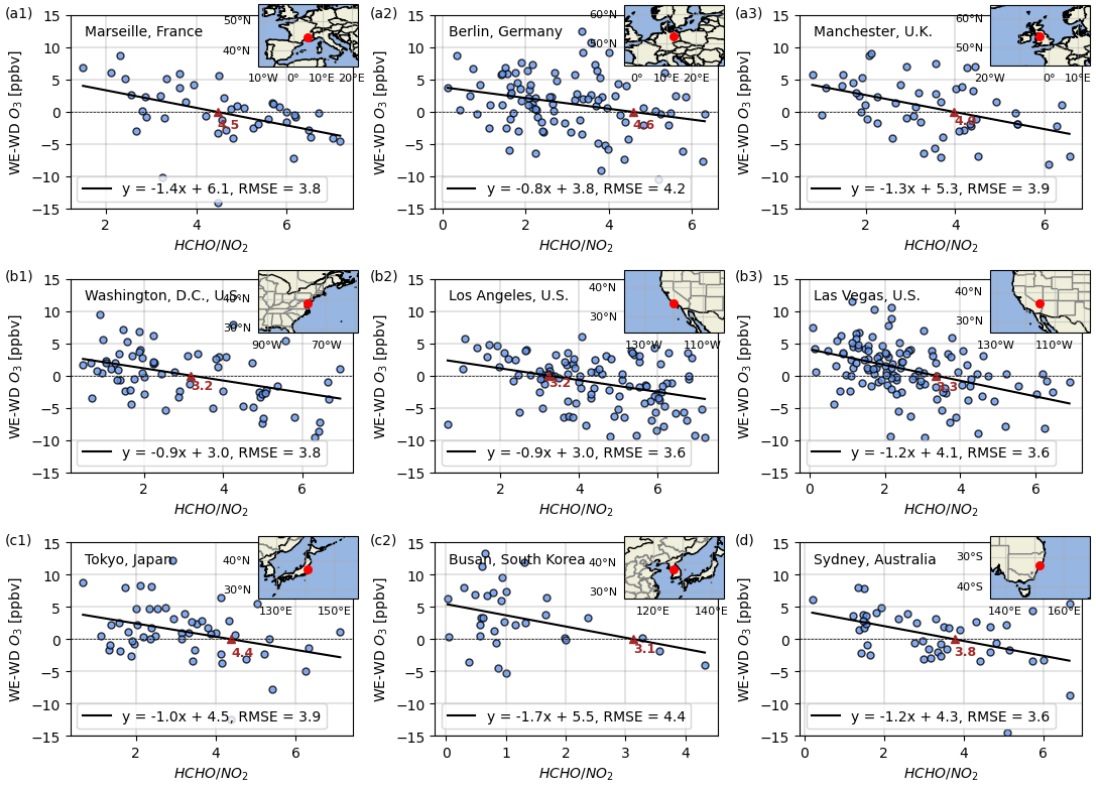

Figure 2: Scatter plot of the monthly average satellite-derived HCHO/NO₂ ratio versus the WE-WD O_3 concentration in 9 representative urban sites from 2004 to 2022. The black line represents the fitted linear regression line. Red triangles denote the intersection points of the regression line with the WE-WD O_3 = 0 baseline.

O_3 formation is a highly nonlinear process in relation to NO_x and VOCs. When urban areas enter weekend, NO_x emissions

https://doi.org/10.5194/egusphere-2025-368
Preprint. Discussion started: 4 February 2025

typically decrease due to reduced commuting and industrial activities (Figure S1). In VOC-limited regime, NO_x reduction leads to increased weekend O_3 levels (positive WE-WD O_3), whereas in NO_x-limited regime, it results in decreased weekend O_3 levels (negative WE-WD O_3). In theory, a transition threshold should exist between these two regimes. Figure 2 illustrates the correlation between monthly mean $HCHO/NO_2$ ratio from satellite data compared to the in-situ WE-WD O_3 in 9 representative metropolitan cities across 4 continents, showing a clear negative correlation and a transition from positive to negative WE-WD O_3 values at a specific $HCHO/NO_2$ ratio. Assuming that O_3 formation differences are attributable to NO_x changes only, $HCHO/NO_2$ value at the WE-WD O_3 = 0 crossing can be considered the threshold separating VOC-limited and NO_x-limited regimes. For example, in Washington, D.C., this key threshold is found to be 3.2 (Figure 2 b1).

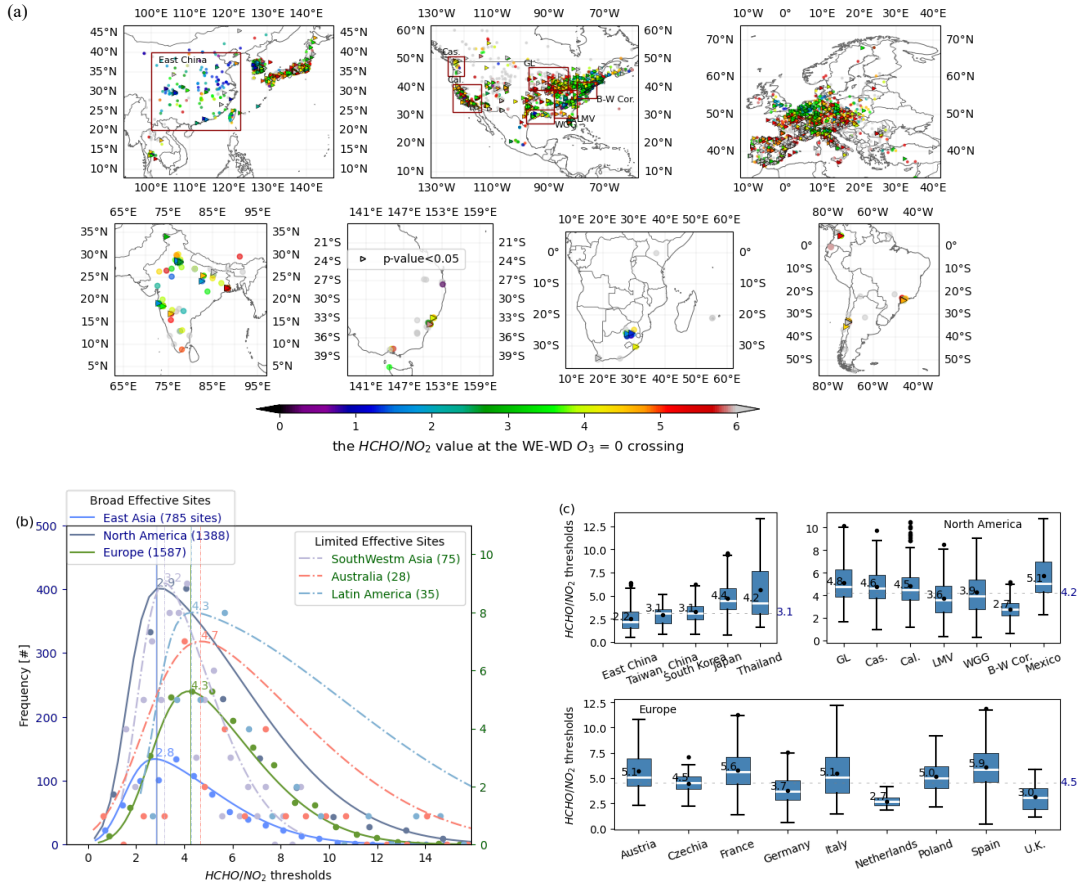

Figure 3: (a) Global map of regime transitional threshold values for $HCHO/NO_2$, derived by assessing the correlation between monthly $HCHO/NO_2$ and WE-WD O_3 difference. We restrict our analysis to ground sites with at least 5 years' observation. Triangles represent sites with linear regression lines fitting within the 95% confidence interval (Wald test for slope, p-value < 0.05). Specific economic regions are highlighted with red rectangles, including: Specific economic regions are highlighted with red rectangles, including: East China; Great Lakes region (GL), Cascadia region (Gas.), California (Cal.), Lower Mississippi Valley region (LMV), West Gulf Coast (WGG), and Boston-Washington Corridor (BW Cor.) in the U.S. (b) Distribution of site numbers across varying threshold bins, with solid/dashed lines representing continents with >100 sites and 20-100 effective sites, respectively. (c) Box plot of thresholds in economically advanced regions of East Asia, North America, and Europe, as marked in (a). The dark-blue numbers on the right axis indicate the median threshold value for all regions presented.

https://doi.org/10.5194/egusphere-2025-368
Preprint. Discussion started: 4 February 2025

By aggregating all TOAR O_3 observations based on corresponding monthly OMI data, we evaluate the thresholds through linear regression between the monthly mean WE-WD O_3 and the $HCHO/NO_2$ ratio at the ground-based sites with at least 5 years' observations. The key thresholds indicating O_3 regime shifts are identified as the critical point where WE-WD O_3 changes sign. The spatial distribution and statistical results of the identified critical points are presented in Figure 3. Globally, robust linear relationships are observed, particularly pronounced in regions such as South Korea, Japan, the U.S., and Europe (Figure 3a), which also have the highest density of monitoring stations. We find a wide distribution of thresholds across different regions (Figure 3b), implying a large spatial variability in the threshold values. Among the sites where the linear regression is statistically significant with p-value < 0.05, approximately 63% of the sites have threshold values between 2 to 5, with over 80% of these sites between 2.5 and 4.7, and the mean value around 3.5. East Asia has the lowest mean threshold value at 2.8 with the minimum over the East China (2.2) and maximum over Japan (4.4) (Figure 3c). In North America, the threshold value is around 2.9, with the eastern seaboard sites averaging 2.7±1 and the sites in western region, predominantly centered in California, slightly higher at 4.5±1, and the maximum value is around 4.8, which is located in the southwest of the Great Lakes region. Europe, with the densest sites of robust linear relationship, has the second-highest critical threshold at 4.3, comparable to Latin America, and just below Australia's 4.7. In Europe, a lower threshold cluster from 2.5 to 3.5 is centered in western Germany, extending to Belgium, northeastern France, the Netherlands, and parts of eastern U.K., with similar low spots in northern Portugal, southern Spain, and northern Italy. Southwest Asia's values are centered around 3.2. Africa and Southeast Asia, with fewer than 20 effective sites (over 5-year continuous observation), are excluded from the analyses due to limited representativeness.

It should be noted that these calculations do not account for the effects of short-term synoptic processes on temperature and the conditions affecting O_3 transport and diffusion. The regime thresholds have uncertainties, and previous studies typically assume a range for regime threshold values (Sillman, 1999; Jin et al., 2020; Jin et al., 2017). This implies that the critical threshold values identified in this study should not be considered definitive indicators that guarantee a regime shift. Nonetheless, this method remains valuable for leveraging large-scale satellite data to track the global progression of O_3 regimes, especially in regions and periods where in-situ O_3 data are limited. We will further explore this using the statistically derived threshold in Section 3.3.

3.2 Long-term Trends and Trend Reversals in Satellite-based $HCHO/NO_2$

Using satellite-based $HCHO/NO_2$ as a determinant for identifying O_3 chemical regimes, we assess the spatial variations and long-term evolution of O_3 chemical regime over global anthropogenic regions from 1996 to 2022. Figure 4 show the multi-year average $HCHO/NO_2$ ratio maps from 1996 to 2022, derived from the harmonized satellite dataset. Notable areas with extremely low $HCHO/NO_2$ ratios of below 1 include East China, Seoul-Suwon region in South Korea, the major urban areas of southern Honshu in Japan, and European regions centered around Belgium, the Netherlands, and eastern United Kingdom, as well as northern Italy. Local minima are found in metropolitan areas such as China's Pearl River Delta, U.S. regions including Los Angeles and San Francisco, urban clusters along the East Coast, and South Africa's Johannesburg etc. These regions are likely under long-term VOC-limited regime. Regions with ratios below 2 include the extensive area of the eastern U.S., the Mumbai and Delhi-New Delhi corridor in India, and major Australian

https://doi.org/10.5194/egusphere-2025-368
Preprint. Discussion started: 4 February 2025

cities like Canberra, Sydney, and Adelaide. The distribution of areas with low HCHO/NO_2 ratio close aligns with that of high NO_2 areas (Figure S2a). NO_x emissions, primarily linked to population density and economic activities, predominantly originate from high-temperature combustion processes involving nitrogen and oxygen, such as industrial emissions and vehicle exhaust (Liu et al., 2016). With its short atmospheric lifetime of a few hours to a day, the distribution of NO_2 reflects hotspots of power generation and fossil fuel consumption (Jamali et al., 2020). In contrast, HCHO, an intermediate in the degradation of various VOCs (De Smedt et al., 2015), exhibits a more uniform distribution due to the widespread biogenic sources of VOCs (Figure S2b).

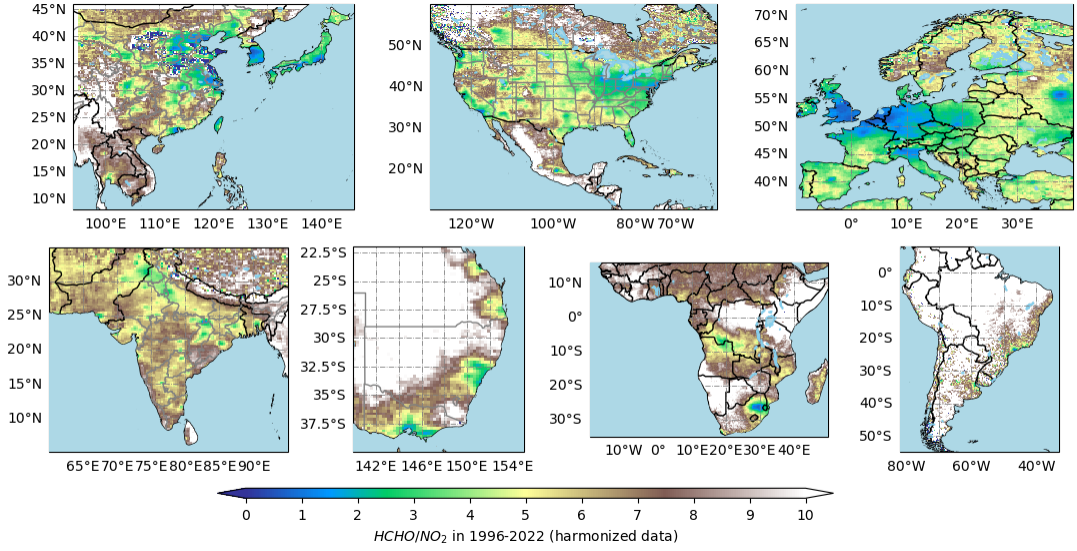

Figure 4: Tropospheric HCHO/NO_2 ratio patterns using the self-consistent GOME, SCIAMACHY and OMI dataset for the combined period 1996 – 2022.

Figure 5 shows the long-term linear trends of tropospheric HCHO/NO_2 ratios from 1996 to 2022. Here we focus on regions with long-term mean tropospheric NO_2 column greater than 1.5×10^{15} molecules/cm^2 and statistically significant trends with p-value < 0.05. Globally, satellite HCHO/NO_2 shows robust linear trends but with diverse directions. In densely populated area, we find positive trend in HCHO/NO_2 over developed nations and a downward trend in HCHO/NO_2 in developing regions. Significant positive trends, averaging 0.11 ± 0.05 yr^{-1}, are observed in Japan and extensive regions of the U.S., particularly along the eastern seaboard and in California. South Korea, the mid-south U.K., north France, Belgium, and part of the Netherlands, Germany, Spain and Italy exhibit a mild decline of 0.04 ± 0.03 yr^{-1}, peaking at 0.12 yr^{-1} in the urban cluster of northeast France. In contrast, central-eastern China, eastern India, show strong negative trends of -0.1 ± 0.05 yr^{-1}, with the steepest declines seen in China's lower Yangtze River region (over -0.18 yr^{-1}) and Kolkata, India (-0.13 yr^{-1}). Weaker negative trends of less than -0.08 yr^{-1} are also seen in eastern Europe near the Black Sea, Melbourne and Sydney, Australia and along northern Algeria's Mediterranean coast in North Africa.

https://doi.org/10.5194/egusphere-2025-368
Preprint. Discussion started: 4 February 2025

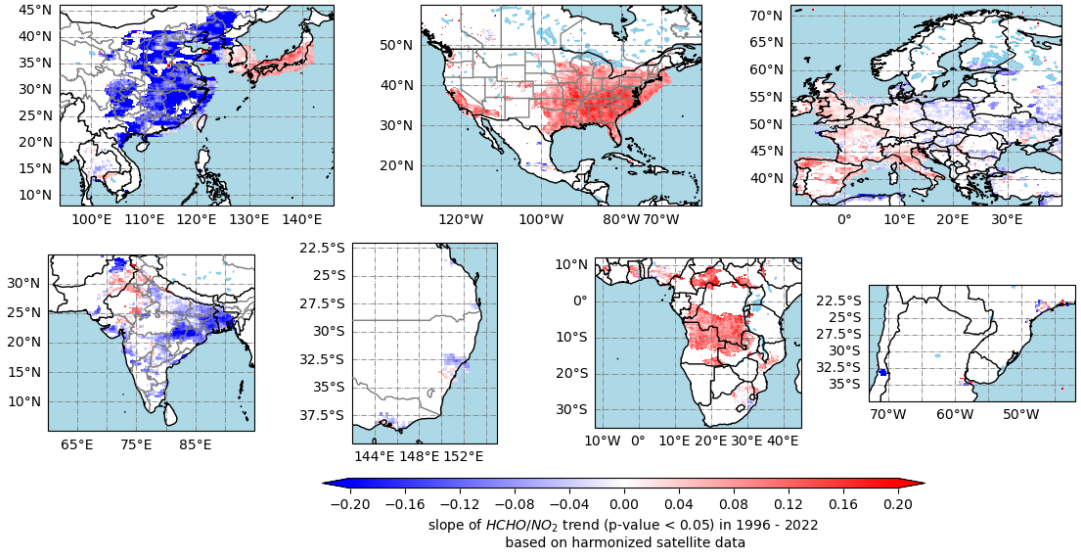

Figure 5: Satellite-based trends of tropospheric HCHO/NO_2 ratios (1996–2022) for grids with a mean NO_2 VCD > 1.5×10^{15} (molecules · cm^{-2}) and statistically significant trends at the 95 % confidence level.

While we apply linear regression to identify the overall trends, trends in Figure 5 could shift due to factors like environmental policies and economic changes etc. These minor trend changes do not affect the linear fit's confidence. However, in certain areas, such as the North China Plain, significant turning points can render the linear fit insignificant. Here, rapid population growth and industrialization were followed by substantial policy-driven reductions in gaseous pollutant emissions, leading to trend reversals that the linear model fails to capture. This indicates that areas appearing blank in Figure 5 are not necessarily trendless but may have sharp turning points.

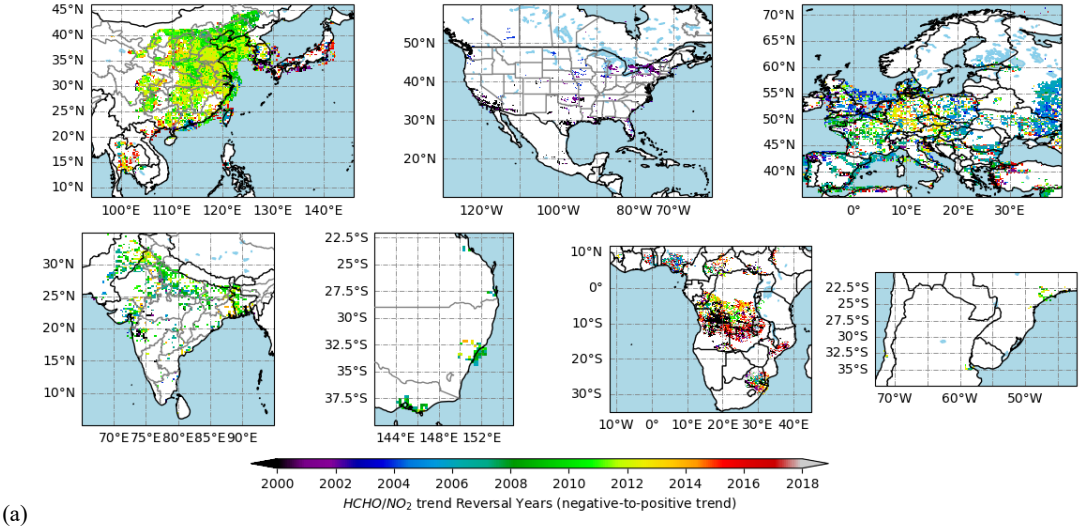

(a)

https://doi.org/10.5194/egusphere-2025-368
Preprint. Discussion started: 4 February 2025

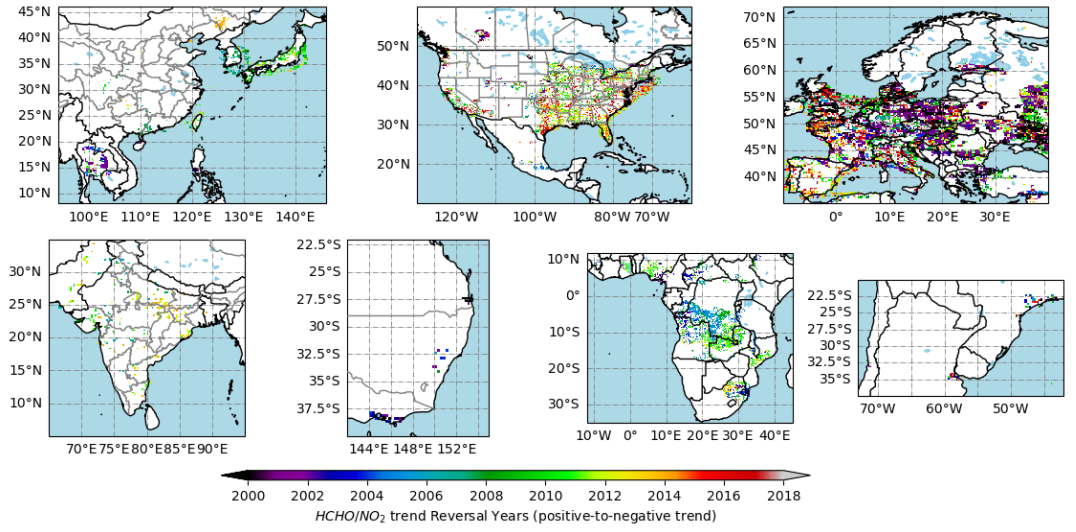

(b)

Figure 6: The year of trend reversals of tropospheric HCHO/NO_2 ratio: (a) from negative to positive and (b) from positive to negative. Only grids with a with a long-term mean tropospheric NO_2 column greater than 1.5×10^{15} molecules/cm^2 and statistically significant trends with p-value < 0.05 for the period before and after the year of reversals are shown.

Next, we assess whether reversals of the trends exist in satellite HCHO/NO_2, using the methods described in Georgoulias et al. (2019). Figure 6 shows our estimated year when a persistent reversal of the trend occurs for HCHO/NO_2. We only include grid cells with statistically significant trends (p-value < 0.05) for both pre- and post-reversal periods. Figure 6a shows the regions where we find trend changes from negative to positive, and Figure 6b shows the regions where the trend transitioned from positive to negative. It should be noted that some regions may experience several reversals, here we only highlight the most significant trend reversals at each grid. The timing of reversals in the HCHO/NO_2 ratio is highly variable across different regions. In Asia, particularly in East China and North India, we observed a single reversal in the HCHO/NO_2 ratio from negative to positive trends around 2011. Conversely, major city clusters in North America exhibit a contrasting trend, with a significant shift from positive to negative trends occurring around 2012-2016. European countries generally display multiple distinct trend reversals. The first occurred in the early 2000s, transitioning from increase to decrease trends, followed by a shift back to positive trends around 2005-2012. Another notable shift to negative trends occurred in central and western European countries between 2015 and 2017. Major urban areas in southeast Australia saw a delayed single negative to positive reversal between 2006 and 2009. Overall, since the 21st century, there has been a notable upsurge in HCHO/NO_2 within the industrialized western world. Till 2015, the U.S. experienced a substantial growth rate of 52-124%, Europe by 12%-17%, and Japan by 77%. From 2015, a minor decline emerged in some U.S. regions, with California being one of the most pronounced, yet not widespread enough to form a significant regional pattern. This reversal correlates with the decline of HCHO and the leveling-off of NO_2 trends (Figure S3a). While meteorological factors can account for the 3-5 years cyclical fluctuations in HCHO/NO_2 ratios, the persistent changes in trends are primarily governed by variations in pollutant emission. In China, the post-2011 decline in HCHO/NO_2 ratio, aligned with the observed national NO_x emission reductions, is largely attributed to NO_x control measures in power plants

https://doi.org/10.5194/egusphere-2025-368
Preprint. Discussion started: 4 February 2025

and industries and stricter vehicle emission standards (China IV) (Van Der A et al., 2017). Changes in VOCs emission also contribute to this rapid increase; according to Liu et al. (2021), from 2011 to 2017, China's industrial VOCs emissions increased from 11122.7 thousand tons/yr to 13397.9 thousand tons/yr. In the U.S., following the implementation of the Clean Air Act Amendments in 1990, the EPA has placed a strong emphasis on the comprehensive assessment of pollutants, moving from an focus on VOCs control to a more integrated strategy that addresses both VOCs and NO_x in the formulation of photochemical pollution control strategies (Amendments, 1990). This shift directly led to the significant reductions in NO_2 levels across the U.S. since 2000, but the trends of HCHO are flat, largely due to the contributions from biogenic VOCs. Between 2000 and 2015, NO_2 levels fell to ~46% and HCHO levels to 92-98% of their initial values (Figure S3). As a result, the long-term trend in $HCHO/NO_2$ over U.S. are dominated by the trends of NO_2.

Within the scope of our study period, NO_2 variations exceeded those of VOCs in the majority of the regions we interested. For these regions, the $HCHO/NO_2$ trend is predominantly influenced by NO_2 trends, with VOC trends showing minor impacts. A distinct negative inflection point observed in the NO_2 trend around 2011 in eastern China and in the early 2000s in the U.S. and Europe supports this (Figure S4). From 1996 to 2022, China's NCP region's NO_2 levels increased fivefold, peaking at eightfold the initial value in 2011, while HCHO levels only rose to 1.5 times the initial value (Figure S3). Europe also showed a more significant changes in NO_2 levels: Europe's NO_2 levels fell to 36-73% and HCHO to 120-133% of 1996 levels. For an in-depth understanding of the factors influencing $HCHO/NO_2$ trends, we refer readers to key literatures on the long-term monitoring of HCHO and NO_2. Specifically, Georgoulias et al. (2019) provided a satellite-based analysis of NO_2 trends from 1996 to 2017, which supports the long-term consistency of our observations, albeit with minor discrepancies in the examined time periods. For a nuanced understanding of HCHO trends, both regional studies (Fan et al., 2023; Kuttippurath et al., 2022) and global perspectives (De Smedt et al., 2008; De Smedt et al., 2015) are instrumental.

Collectively, by combining linear fitting and reversals analysis, we discern a predominant positive global trend in the $HCHO/NO_2$ ratio, or a shift from negative to positive in the past 27 years, with distinct regional variations. Developing regions like East China and North India, which have relatively late economic development and pollution control measures, typically show twice trend reversals. In contrast, developed regions such as North America and Europe, where $HCHO/NO_2$ ratios began to increase significantly in the early 2000s exhibit a more consistent upward trend. Although these developed areas have experienced minor downward reversals or stagnation in recent years due to the rate of NO_x reduction slowing down.

3.3 Global Transitions in O_3 Chemical Regimes Delineated by Satellite-Derived $HCHO/NO_2$ Ratios

As elaborated in Section 3.1, the correlation between the $HCHO/NO_2$ ratio and the WE-WD O_3 response patterns show similarities but also small variations across different regions. Here, for simplicity, we apply a uniform global threshold of $HCHO/NO_2$=3.5 to explore potential years of O_3 regimes changes. To describe how the O_3 chemical regime has evolved, we categorize into four main categories based on the long-term trends of $HCHO/NO_2$ (Table 1): (1) constant O_3 chemical regimes: regions with a single VOC-limited or NO_2-limited regime status without regime transition during the study

https://doi.org/10.5194/egusphere-2025-368
Preprint. Discussion started: 4 February 2025

period; (2) constant quasi regime: regions with single regime for most of the time but has potential to exceed the threshold value of 3.5; (3) single shift of the regime: regions with single shift, either from VOC-limited to NO_x-limited, or vice versa; (4) multiple shifts of the regime: regions with nonlinear trends in $HCHO/NO_2$, in which a reversal of the trends in $HCHO/NO_2$ is identified, and $HCHO/NO_2$ crosses over the threshold values at least once. This classification takes into account the initial conditions of O_3 regimes and their transitional characters based on the observed $HCHO/NO_2$ trend. Here, we examine the O_3 regime changes based on annual average $HCHO/NO_2$, but the O_3 chemical regime should vary seasonally (Jin et al., 2017; Jacob et al., 1995), typically becoming more NO_x-saturated in wintertime and more NO_x-limited in summertime. We do not account for the seasonality of O_3 production regimes because the definitions of seasons vary by climate regions would complicate the comparisons across different regions.

Table 1: Criteria for distinguishing different types of O_3 regime transitions.

Category	Subcategory	Description of $HCHO/NO_2$ Trend Pattern	Transition Year
Constant regimes	1.1 fixed NO_x-limited	Typical NO_x-limited condition ($HCHO/NO_2 \geq 4.5$) for 80% of the period.	No regime transition
	1.2 fixed VOC-limited	Typical NO_x-saturated condition ($HCHO/NO_2 \leq 2.5$) for 80% of the period.	
Constant quasi regimes	2.1 fixed quasi-NO_x-limited	$HCHO/NO_2$ ratio within 3.5 - 4.5 for 80% of the period, with the possibility of exceeding 4.5 but never falling below 3.5.	
	2.2 fixed quasi-VOC-limited	$HCHO/NO_2$ ratio within 2.5 - 3.5 for 80% of the period, with the possibility of falling below 2.5 but never exceeding 3.5.	
Linear trend with regime transition	3.1 shift from VOC-limited to NO_x-limited	positive $HCHO/NO_2$ trend (↗) and crosses the $HCHO/NO_2 = 3.5$.	Intersection with $HCHO/NO_2 = 3.5$
	3.2 shift from NO_x-limited to VOC-limited	negative $HCHO/NO_2$ trend (↘) and crosses the $HCHO/NO_2 = 3.5$.	
Non-linear trend with regime transition	3.3 shift from VOC-limited to NO_x-limited	For negative to positive trend (↘↗): $HCHO/NO_2$ crosses 3.5 after the reversal year	
		For positive to negative trend (↗↘): $HCHO/NO_2$ crosses 3.5 before the reversal year	
	3.4 shift from NO_x-limited to VOC-limited	For negative to positive trend (↘↗): $HCHO/NO_2$ crosses 3.5 before the reversal year	

https://doi.org/10.5194/egusphere-2025-368
Preprint. Discussion started: 4 February 2025

		For positive to negative trend (↗↘): $HCHO/NO_2$ crosses 3.5 after the reversal year

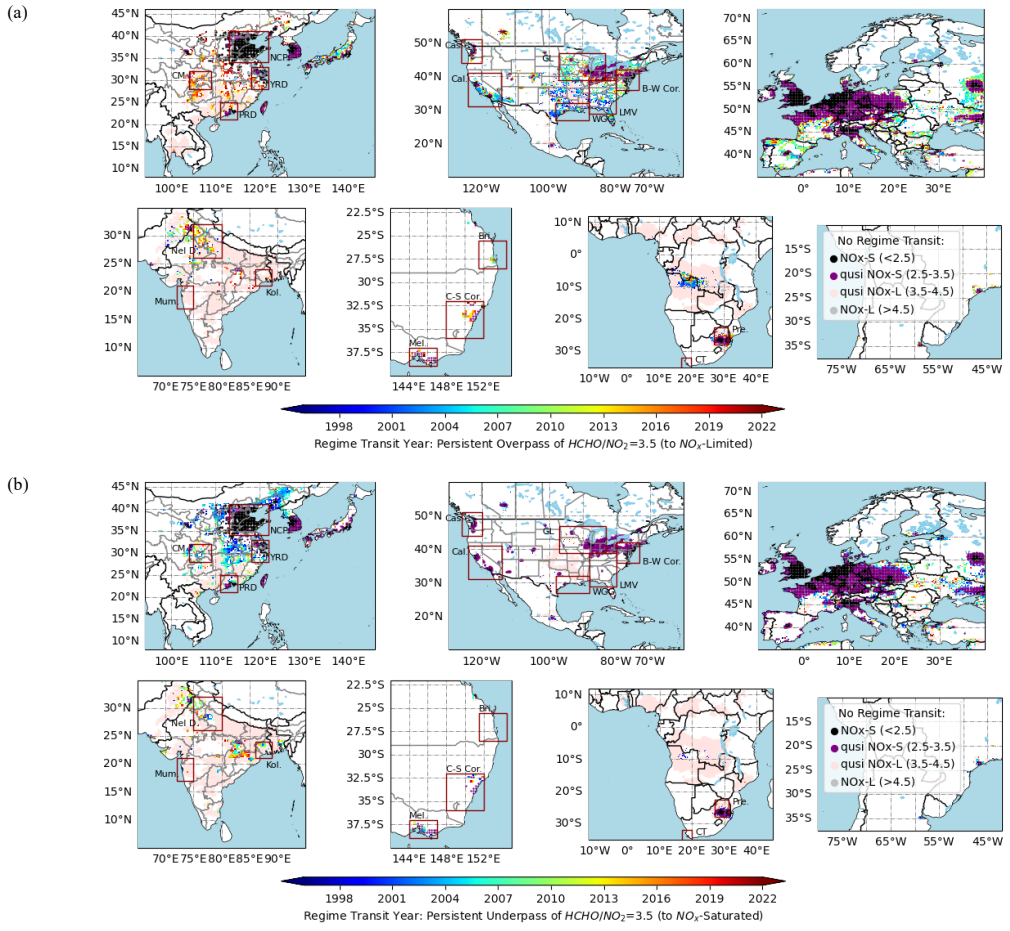

Figure 7: Estimated transition year of O_3 regimes: grids where the annual $HCHO/NO_2$ ratio exceeds 3.5 (a) with a positive annual trend, and (b) with a negative annual trend. Only grids with a with a long-term mean NO_2 VCD > 1.5×10^{15} ($molecules \cdot cm^{-2}$) are shown. Specific economic regions are highlighted with red rectangles, including: Specific economic regions are highlighted with red rectangles same as Figure 3a, adding: North China Plain (NCP), Yangtze River Delta (YRD), Pearl River Delta (PRD), and Chongqing Municipality (CM) in China; New Delhi (Nel D.), Mumbai (Mum.), and Kolkata (Kol.) in India; Melbourne (Mel.), Capital-Sydney Corridor (C-S Cor.), and Brisbane (Bri.) in Australia; Pretoria (Pre.) and Cape Town (CT) in South Africa.

Figure 7 shows the classification of the regime changes. Globally, $HCHO/NO_2$ has shown a general upward trend post-2011, yet many central economic zones remain VOC-limited or quasi-VOC-limited, with the $HCHO/NO_2$ ratio not exceeding the threshold of 3.5 (Figures 7 and 8). Key regions, including China's NCP, YRD and PRD, Seoul in South Korea, Japan's metropolitan areas, the U.S. East Coast and California's Los Angeles and San Francisco areas, parts of

https://doi.org/10.5194/egusphere-2025-368
Preprint. Discussion started: 4 February 2025

335 center-western Europe, India's New Delhi, South Africa's Pretoria and Cape Town region have been consistently VOC-limited for the majority of period (over 80%) since1996. India, with its unique climate and emissions profile, exhibits a large area in the quasi-NO_x-limited range (3.5-4.5). India's hot and humid climate contributes to elevated BVOC and HCHO emissions (Kuttippurath et al., 2022), reducing NO_x lifetime and accumulation, which tends to be more NO_x-limited. We observe an urban-rural transition from VOC-limited to NO_x-limited in megacity clusters, with the periphery
340 zones showing the initial shift toward NO_x-limited, progressing inward. This pattern is particularly evident in megacities such as Tokyo, San Francisco and Los Angeles. Regions have extensively transitioned to the typical NO_x-limited stage include the middle parts of Honshu in Japan, south California, parts of eastern U.S., and various regions in Europe.

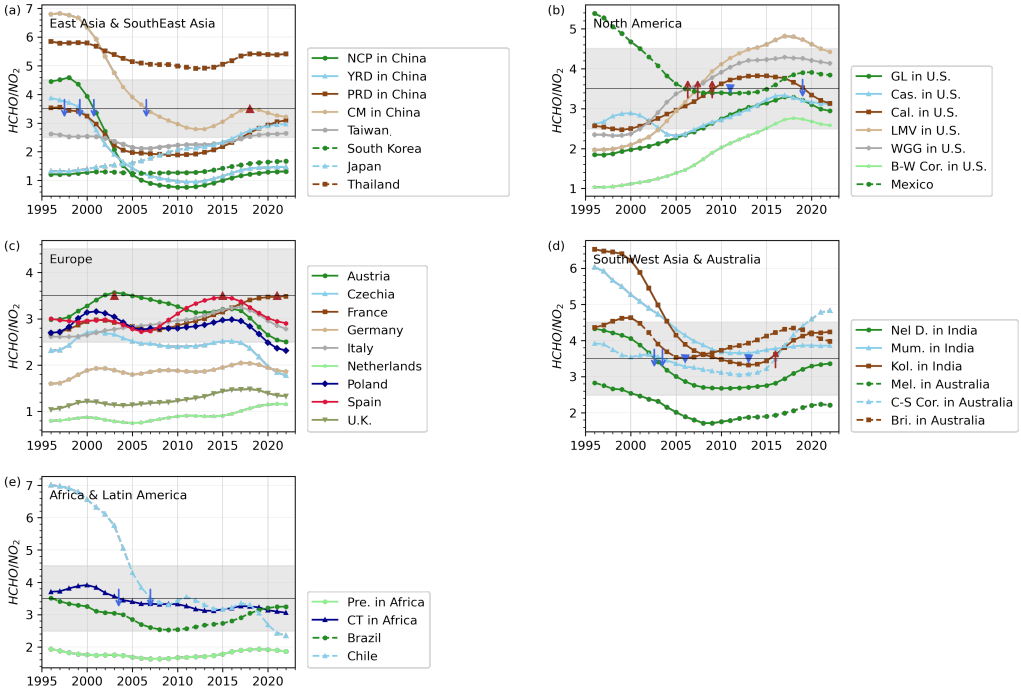

345 **Figure 8: Long-term trends of tropospheric $HCHO/NO_2$ ratio across major economic regions marked in Figure 7 based on the harmonized satellite data. Here we only focus on grid cells with long-term mean tropospheric NO_2 column greater than 1.5 × 10^{15} molecules/cm^2. The arrow lines depict the intersection points with $HCHO/NO_2$=3.5.**

Figure 8 shows the long-term evolution of the satellite-based $HCHO/NO_2$ in different sub-regions of the world. The temporal evolution of regional O_3 regimes is intricately tied to a variety of emission policies, economic development, and geographical characteristics, such as surface coverage and regional meteorological conditions. Nations that embarked on
350 industrialization and VOCs reduction policies early on, like the U.S., Japan, and European countries, were predominantly in VOC-limited regime ($HCHO/NO_2$<2.5) by 1996 and have since shown a significant increasing trend in the $HCHO/NO_2$ ratio, particularly post-2000. Although most regions in the U.S. and some European countries (e.g., France, Germany, and Italy etc.) have reached peak levels around 2015-2017 and are currently experiencing a plateau or modest decline in the $HCHO/NO_2$ ratio, this has not significantly altered the overall upward trajectory of the ratio over the past 27 years. A

https://doi.org/10.5194/egusphere-2025-368
Preprint. Discussion started: 4 February 2025

few regions have surpassed critical thresholds to NO_x-limited conditions—most notably observed in the southeast U.S. between 2006 and 2010—while most have yet to reach the 3.5 thresholds, either remaining in the typical VOC-limited (e.g., South Korea, China's NCP, YRD, etc.) or O_3 transitional regime (e.g., most regions in the U.S.). In regions that have attained $HCHO/NO_2$>3.5, such as the LMV, WGG, and California in the U.S., the post-peak decline did not cause a secondary transition point causing an O_3 regime shift. California, for example, surpassed the key threshold around 2009 and reached a maximum value within the quasi-NO_x-limited range by 2014, showing a re-crossing of the threshold around 2018, but still within the transitional regime.

Economies with relatively late industrial takeoffs, such as those in East China and India, initially had a high $HCHO/NO_2$ ratio around 1996, indicating NO_x-limited condition. As these economies bloomed in the late 1990s, NO_x emissions from fuel combustion caused a sharp decline in the $HCHO/NO_2$ ratio, particularly in 2000-2005 period. In eastern China, the NCP and YRD regions saw a rapid decrease in the $HCHO/NO_2$ ratio (-0.56/year), dropping from ~4 in 2000 to ~1.2 in 2005 (Figure 8a). Post-2005, the decline rate slowed, and by 2011, a slow reversal (<0.1/year) began, but it still remains in a VOC-limited regime to date. In contrast, Indian cities like Mumbai and Kolkata experienced a rapid decline in the $HCHO/NO_2$ ratio since 2000, but have not significantly crossed the key threshold (Figure 8d). In the Southern Hemisphere, regions like Australia, Africa and Latin America, typically exhibit low NO_x emissions (< 1.5×10^{15} molecules/cm^2) across vast areas due to the highly uneven population distribution. Melbourne's $HCHO/NO_2$ trend reversed around 2008, varying within a VOC-limited range of 1.8 to 2.8. The Canberra-Sydney corridor and Brisbane area show higher ratios (3.1 to 4.8) with no regime change throughout the observation period (Figure 8d). In Africa, the Pretoria region and Cape Town in South Africa exhibit a slow annual decrease of <-0.02/year (Figure 8e), averaging around 1.8 and 2.8. Latin American megacities have also remained in a transitional regime over the past two decades. These observations highlight the complexity of O_3 regime patterns and the significant influence of region-specific factors.

Note that the regime threshold values are subject to large uncertainties due to factors such as meteorological conditions and satellite detection noise (Jin et al., 2017; Souri et al., 2017; Souri et al., 2020; Schroeder et al., 2017). The key $HCHO/NO_2$ threshold of 3.5 used here is derived from observation sites from TOAR network, which tend to be in urban or accessible areas, which is more reflective of regions with significant human impact rather than pristine natural environments. These factors have the potential to bias the estimated transition year. However, such bias is not significant. It is estimated that a ~10% variation in the threshold (e.g., from 3.5 to 3.9) would shift the estimated transition years by only about 1-2 years for the major global regions. The uncertainty introduced by this simplified approach is considered acceptable and does not compromise the analysis's effectiveness in pinpointing critical transition years.

3.4 O_3 Regime Transition Consistent with Diminishing O_3 Weekend Effect

Over the past 2 decades, a significant reduction in NO_2 concentrations is found (Figure S3). Despite this trend, weekend NO_2 levels remain lower than those on weekdays (WE-WD NO_2<0) in most areas, although this NO_2-weekend-low phenomenon is weakening (Figure S1). Differential NO_x saturation levels influence O_3 sensitivity to NO_x, resulting in varying WE-WD O_3 patterns. The interannual evolution in these patterns, in terms of sign and magnitude, provides another

https://doi.org/10.5194/egusphere-2025-368
Preprint. Discussion started: 4 February 2025

piece of evidence of O_3 regimes changes. Figure 9 shows a spatial overview of the WE-WD O_3 differences across three distinct periods (2004 – 2013, 2014 – 2018, 2019 - 2023) over the past two decades. Figure 10 shows the long-term O_3 weekend effect averaged across the sites. For robust statistical analysis, continental regional-averaged trends are limited to sites with at least 10 years of data, focusing on East Asia, North America, Europe, and Latin America.

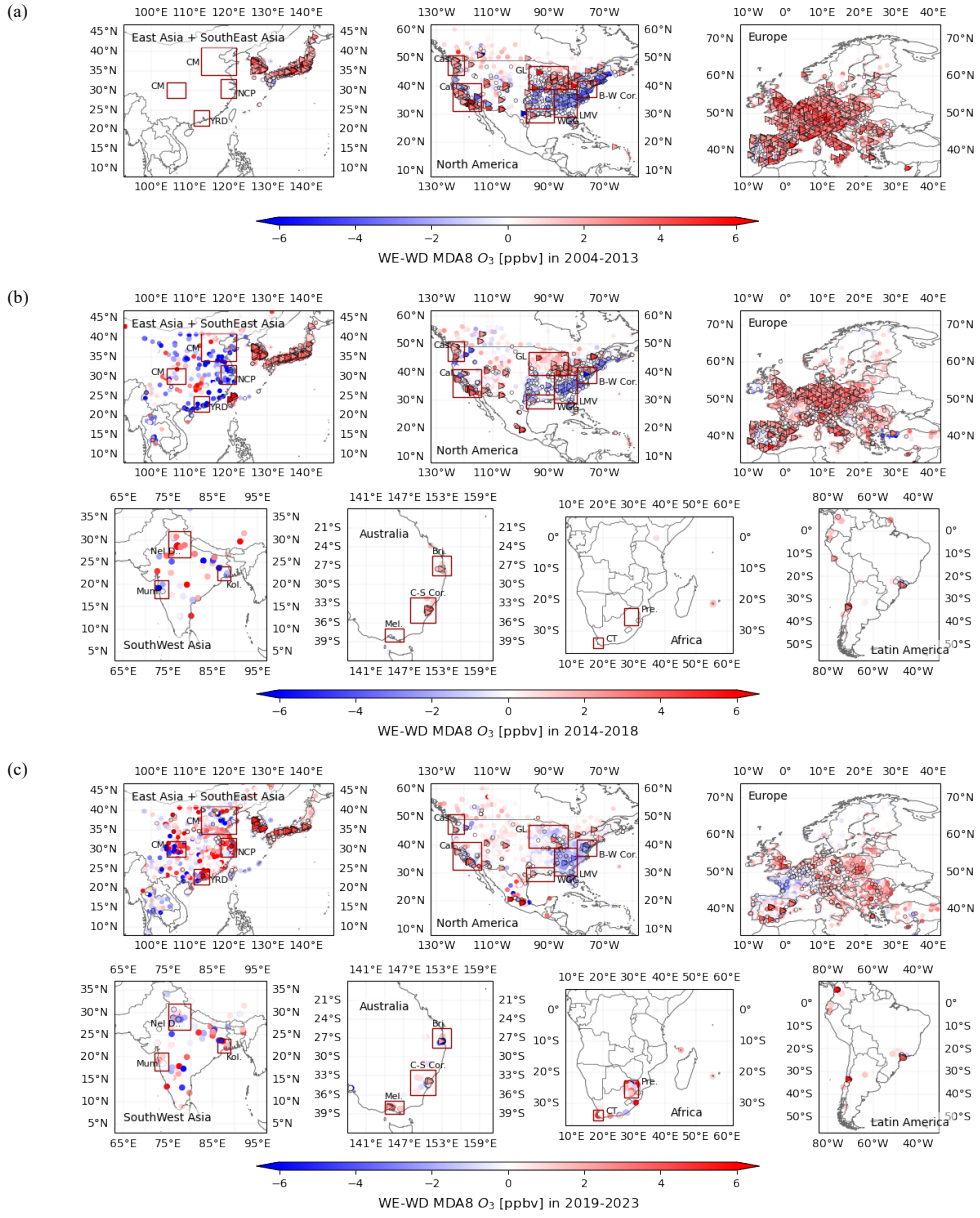

Figure 9: Two-decade evolution of WE-WD O_3 differences across three distinct period: (a) 2004-2013, (b) 2014-2018, (c) 2019-2023. Significant (p-value of t-test < 0.05) WE-WD O_3 difference and WE-WD NO_2 differences are denoted by triangles and

https://doi.org/10.5194/egusphere-2025-368
Preprint. Discussion started: 4 February 2025

395 **black-edged symbols respectively.**

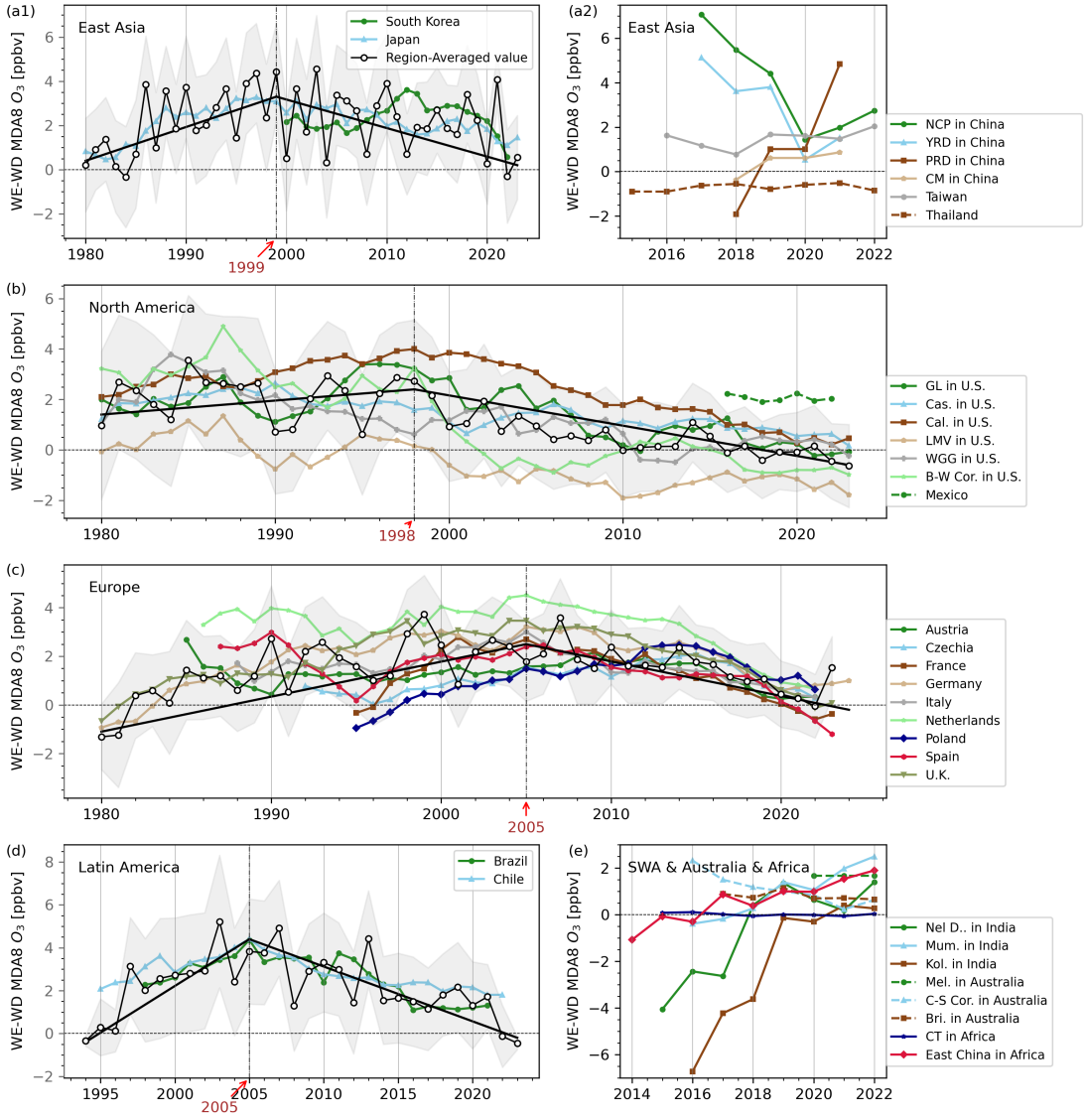

Figure 10: Long-term evolution WE-WD O_3 difference derived from TOAR ground-based O_3 observation. Only sites with >=10 years of data are included in the continental region-averaged statistics (black line), and sites with >=3 years of data are included in the major economic regions and selected countries statistics.

400 The WE-WD O_3 trend is inversely correlated with the HCHO/NO_2 ratio, showing an initial rise followed by a decline since 1980, with meteorological-driven interannual fluctuations observed throughout the period. The inflection points vary across different regions, generally occurring within the decade between 1995 and 2005 (Figure 10). The Theil-Sen slope, calculated from the most recent two decades of data, reveals a significant and widespread negative trend in WE-

https://doi.org/10.5194/egusphere-2025-368
Preprint. Discussion started: 4 February 2025

WD O_3 concentrations at the majority of global monitoring sites, with a robust trend significance (p-value <0.05) confirmed by the Mann-Kendall test, especially in North America, Europe, Japan, South Korea, and developed regions of Australia and Latin America (Figure S4). In Europe, before 2013, over 70% of TOAR sites demonstrated significant weekend O_3 increases (Figure 9a); by 2019-2023, only 2% of sites continued to show significant weekend elevations (Figure 9c). The ensembled time series of Europe sites indicates that the peak WE-WD O_3 occurred around 2005, at approximately 2.5 ± 1.1 ppbv, whereas by 2023, it had significantly decreased to near zero (Figure 10c). Similar reductions have been observed in the U.S., with the largest WE-WD O_3 occurring between 1995 and 2000, and the most substantial differences noted in California around 1998, peaking at approximately 4 ppbv (Figure 10b). In East Asia, where long-term O_3 observations spanning over a decade are confined to Japan and South Korea, the aggregated data from monitoring sites indicated a notable annual maximum around 1999, registering 3.3 ± 0.5 ppbv (Figure 10a1). This value is more reflective of Japan's data, given that South Korea's monitoring began in 2000, with its own maximum occurring around 2012.

In Latin America, developed countries such as Brazil and Chile observed their peaks around 2005, with values around 4 ppbv (Figure 10d). In China and India, extensive ground-based O_3 monitoring networks were established within the last decade. Eastern China, encompassing the NCP and YRD super urban agglomerations, aligns with the global trend of reduced weekend O_3 (Figure 10a2). In India, however, rapidly developing areas such as New Delhi, Mumbai, and Kolkata are experiencing a rise in WE-WD O_3, indicating a complex interaction between emissions and atmospheric dynamics (Figure 10e). Note that due to short observation periods and moderate statistical significance (p-values between 0.05 and 0.1 from the Mann-Kendall test) (Figure S5), results from China and India are best used for qualitative analysis only.

By 2023, a few regions show a reversal of O_3 weekend effect on annual basis. The U.S. LMV area, which first showed a WE-WD O_3 transition to negative values, has kept WE-WD O_3 levels around -1 ± 0.5 ppbv since 2010 (Figure 10b). France and Spain have also shown slightly higher weekend O_3 levels from 2020, but not significant (Figure 10c). Sporadic sub-zero WE-WD O_3 in areas such as parts of California, the BW and WGG regions in the U.S. indicate a potential move towards NO_x-limited conditions, though inconsistent.

Overall, the O_3 weekend effect's long-term changes are consistent with the weakening VOC-limited conditions outlined in Section 3.3, with most regions classified as VOC-limited or in transition. This is evident in the fact that, in most regions, weekend O_3 levels are slightly higher than or equal to those on weekdays. These results are consistent with the satellite-derived $HCHO/NO_2$ observations, indicating a still ongoing transition in the O_3 chemical regime.

4 Conclusion

In this study, satellite-derived $HCHO/NO_2$ ratios and ground-based O_3 observations were directly connected to capture the nonlinearity of global shifts in O_3 chemical regimes. Key findings are as follows:

The evolution of O_3 regimes is discernible through the analysis of $HCHO/NO_2$ ratio and WE-WD O_3 trends. We have

https://doi.org/10.5194/egusphere-2025-368
Preprint. Discussion started: 4 February 2025

pinpointed distinct regional thresholds—2.8 for East Asia, 3.2 for Southwest Asia, 3.0 for North America, 4.3 for Europe and Latin America, and 4.7 for Australia—that signify the pivotal transition points in O_3 regimes. These thresholds are shaped by variations in regional energy profiles, meteorological patterns etc.

Amidst the ongoing changes in the ratios of O_3 precursors, a global trend towards NO_x-limited O_3 regimes have emerged over the past two decades. This is evidenced by both the rising $HCHO/NO_2$ ratios and the diminishing O_3 weekend effect, particularly in densely populated regions. Applying linear fitting and reversals analysis, we've observed a predominant positive or negative-to-positive shift global trend in the $HCHO/NO_2$ ratio over the past 27 years. Later-industrializing regions like East China and India initially saw a decline before rebounding around 2011; industrialized nations like the U.S., Europe, and Japan experienced significant increases in the $HCHO/NO_2$ ratio from the early 2000s due to substantial NO_x emission reductions. However, by 2023, most urban regions' annual-mean $HCHO/NO_2$ ratios have not significantly surpassed the 3.5 threshold, indicating they remain within VOC-limited or transitional regimes. However, O_3 chemical regime varies seasonally, and we expect the regime transition has occurred during the warm season when O_3 pollution is highest. Regarding WE-WD O_3, while some regions like France and northern Spain show lower weekend levels, the majority still report slightly higher weekend O_3 on annual basis, but not statistically significant anymore. A few areas, such as the southeastern U.S., heavily influenced by BVOCs, have clearly entered an NO_x-limited regime on the annual basis. These results align with the general trend of weakening VOC-limited conditions。

The transitional zone for O_3 regimes should be a range rather than a fixed $HCHO/NO_2$ ratio. Our study simplifies this by using the central value of this range, acknowledging a limitation. Despite this, our findings provide valuable insights, highlighting the need for adaptable emission controls in response to atmospheric changes. Early industrialized nations could benefit from policies addressing both NO_x and VOCs to further curb O_3, while later industrializers should prioritize NO_x controls to prevent excessive O_3 formation.

Acknowledgement

Support for this project was provided by NASA Aura Science Team and Atmospheric Composition Modeling and Analysis Program (grant number: 80NSSC23K1004). This research used the computational cluster resource provided by the Office of Advanced Research Computing (OARC) at Rutgers, The State University of New Jersey. We are grateful to the many scientists who contributed to the GOME, GOME-2, SCIAMACHY, OMI and TROPOMI instruments and products.

Data Availability

Multi-satellite products (GOME, SCIMACHY, OMI) of tropospheric NO_2 and HCHO vertical columns are developed under the EU FP7-project Quality Assurance for Essential Climate Variables (QA4ECV) are publicly available at https://knmi.sitearchief.nl/?subsite=qa4ecv#archive. TROPOMI NO_2 data (https://doi.org/10.5270/S5P- s4ljg54) and TROPOMI HCHO (https://doi.org/10.5270/S5P-vg1i7t0) are available from NASA Goddard Earth Sciences (GES) Data

https://doi.org/10.5194/egusphere-2025-368
Preprint. Discussion started: 4 February 2025

and Information Services Center (DISC, https://disc.gsfc.nasa.gov/datasets/). Ground-based O_3 observations are available from TOAR-II database (https://toar-data.org/surface-data). The harmonized annual satellite-based HCHO and NO_2 products will be made publicly available at the publication stage.

Author contribution

Y.T.: Methodology, Formal Analysis, Investigation, Visualization, Writing - Original Draft. **S.W:** Data Collection of Satellite NO_2 products. **X.J.:** Conceptualization, Supervision, Methodology, Data Curation, Funding Acquisition, Writing - Review & Editing. All authors have given approval to the final version of the manuscript.

Competing interests

The authors decline that they have no conflict of interest.

References

Adame, J. A., Hernández-Ceballos, M. Á., Sorribas, M., Lozano, A., and De la Morena, B. A.: Weekend-Weekday Effect Assessment for O_3, NOx, CO and PM10 in Andalusia, Spain (2003–2008), Aerosol and Air Quality Research, 1862–1874, 10.4209/aaqr.2014.02.0026, 2014.

Amendments, C. A. A.: Clean Air Act Amendments of 1990, Pub. L. No. 101-549, 104 Stat. 2399, 1990.

Atkinson-Palombo, C. M., Miller, J. A., and Balling, R. C. J.: Quantifying the ozone "weekend effect" at various locations in Phoenix, Arizona, Atmospheric Environment, 40, 7644-7658, 10.1016/j.atmosenv.2006.05.023, 2006.

Boersma, K. F., Eskes, H., Richter, A., De Smedt, I., Lorente, A., Beirle, S., Van Geffen, J., Peters, E., Van Roozendael, M., and Wagner, T.: QA4ECV NO_2 tropospheric and stratospheric column data from OMI [Data set], Royal Netherlands Meteorological Institute (KNMI). http://www.qa4ecv.eu/ecv/NO_2-pre/data 10.21944/qa4ecv-NO_2-omi-v1.1, 2017a.

Boersma, K. F., Eskes, H., Richter, A., De Smedt, I., Lorente, A., Beirle, S., Van Geffen, J., Peters, E., Van Roozendael, M., and Wagner, T.: QA4ECV NO_2 tropospheric and stratospheric column data from GOME [Data set], Royal Netherlands Meteorological Institute (KNMI). http://www.qa4ecv.eu/ecv/NO_2-pre/data, 10.21944/qa4ecv-NO_2-gome-v1.1, 2017b.

Boersma, K. F., Eskes, H. J., Richter, A., De Smedt, I., Lorente, A., Beirle, S., van Geffen, J. H. G. M., Zara, M., Peters, E., Van Roozendael, M., Wagner, T., Maasakkers, J. D., van der A, R. J., Nightingale, J., De Rudder, A., Irie, H., Pinardi, G., Lambert, J.-C., and Compernolle, S. C.: Improving algorithms and uncertainty estimates for satellite NO₂ retrievals: results from the quality assurance for the essential climate variables (QA4ECV) project, Atmospheric Measurement Techniques, 11, 6651-6678, 10.5194/amt-11-6651-2018, 2018.

CARB: The Ozone Weekend Effect in California. , Planning and Technical Support Division, Sacramento 2003., 2003.

Cermak, J., Wild, M., Knutti, R., Mishchenko, M. I., and Heidinger, A. K.: Consistency of global satellite-derived aerosol and cloud data sets with recent brightening observations, Geophysical Research Letters, 37, 10.1029/2010gl044632, 2010.

https://doi.org/10.5194/egusphere-2025-368
Preprint. Discussion started: 4 February 2025

Chiu, Y. M., Wilson, A., Hsu, H. L., Jamal, H., Mathews, N., Kloog, I., Schwartz, J., Bellinger, D. C., Xhani, N., Wright, R. O., Coull, B. A., and Wright, R. J.: Prenatal ambient air pollutant mixture exposure and neurodevelopment in urban children in the Northeastern United States, Environ Res, 233, 116394, 10.1016/j.envres.2023.116394, 2023.

Choi, Y., Kim, H., Tong, D., and Lee, P.: Summertime weekly cycles of observed and modeled NO and O_3 concentrations as a function of satellite-derived ozone production sensitivity and land use types over the Continental United States, Atmospheric Chemistry and Physics, 12, 6291-6307, 10.5194/acp-12-6291-2012, 2012.

Cleveland, W. S., Graedel, T. E., Kleiner, B., and Warner, J. L.: Sunday and workday variations in photochemical air pollutants in new jersey and new york, Science, 186, 1037-1038, 10.1126/science.186.4168.1037, 1974.

De Smedt, I., Müller, J. F., Stavrakou, T., van der A, R., Eskes, H., and Van Roozendael, M.: Twelve years of global observations of formaldehyde in the troposphere using GOME and SCIAMACHY sensors, Atmospheric Chemistry and Physics, 8, 4947-4963, 10.5194/acp-8-4947-2008, 2008.

De Smedt, I., YU, H., Richter, A., Beirle, S., Eskes, H., Boersma, K. F., Van Roozendael, M., Van Geffen, J., Wagner, T., Lorente, A., and Peters, E.: QA4ECV HCHO tropospheric column data from OMI [Data set], Royal Belgian Institute for Space Aeronomy. http://www.qa4ecv.eu/ecv/hcho-p/data, 10.18758/71021031, 2017.

De Smedt, I., Stavrakou, T., Hendrick, F., Danckaert, T., Vlemmix, T., Pinardi, G., Theys, N., Lerot, C., Gielen, C., Vigouroux, C., Hermans, C., Fayt, C., Veefkind, P., Müller, J. F., and Van Roozendael, M.: Diurnal, seasonal and long-term variations of global formaldehyde columns inferred from combined OMI and GOME-2 observations, Atmospheric Chemistry and Physics, 15, 12519-12545, 10.5194/acp-15-12519-2015, 2015.

Duncan, B. N., Yoshida, Y., Olson, J. R., Sillman, S., Martin, R. V., Lamsal, L., Hu, Y., Pickering, K. E., Retscher, C., Allen, D. J., and Crawford, J. H.: Application of OMI observations to a space-based indicator of NOx and VOC controls on surface ozone formation, Atmospheric Environment, 44, 2213-2223, 10.1016/j.atmosenv.2010.03.010, 2010.

Fan, J., Wang, T., Wang, Q., Ma, D., Li, Y., Zhou, M., and Wang, T.: Assessment of HCHO in Beijing during 2009 to 2020 using satellite observation and numerical model: Spatial characteristic and impact factor, Sci Total Environ, 894, 165060, 10.1016/j.scitotenv.2023.165060, 2023.

Felzer, B. S., Cronin, T., Reilly, J. M., Melillo, J. M., and Wang, X.: Impacts of ozone on trees and crops, Comptes Rendus. Géoscience, 339, 784-798, 10.1016/j.crte.2007.08.008, 2007.

Fu, T. M., Jacob, D. J., Palmer, P. I., Chance, K., Wang, Y. X., Barletta, B., Blake, D. R., Stanton, J. C., and Pilling, M. J.: Space-based formaldehyde measurements as constraints on volatile organic compound emissions in east and south Asia and implications for ozone, Journal of Geophysical Research: Atmospheres, 112, 10.1029/2006jd007853, 2007.

Georgoulias, A. K., van der A, R. J., Stammes, P., Boersma, K. F., and Eskes, H. J.: Trends and trend reversal detection in 2 decades of tropospheric NO_2 satellite observations, Atmospheric Chemistry and Physics, 19, 6269-6294, 10.5194/acp-19-6269-2019, 2019.

GOV.UK: Emissions of air pollutants in the UK – Nitrogen oxides (NOx), 2024.

Jacob, D. J., Horowitz, L. W., Munger, J. W., Heikes, B. G., Dickerson, R. R., Artz, R. S., and Keene, W. C.: Seasonal transition from NOx- to hydrocarbon-limited conditions for ozone production over the eastern United States in September, Journal of Geophysical Research, 100, 9315-9324, 10.1029/94jd03125, 1995.

https://doi.org/10.5194/egusphere-2025-368
Preprint. Discussion started: 4 February 2025

Jaffe, D. A., Ninneman, M., and Chan, H. C.: NO(x) and O(3) Trends at U.S. Non-Attainment Areas for 1995-2020: Influence of COVID-19 Reductions and Wildland Fires on Policy-Relevant Concentrations, J Geophys Res Atmos, 127, e2021JD036385, 10.1029/2021JD036385, 2022.

Jamali, S., Klingmyr, D., and Tagesson, T.: Global-Scale Patterns and Trends in Tropospheric NO_2 Concentrations, 2005–2018, Remote Sensing, 12, 10.3390/rs12213526, 2020.

Jin, X. and Holloway, T.: Spatial and temporal variability of ozone sensitivity over China observed from the Ozone Monitoring Instrument, Journal of Geophysical Research: Atmospheres, 120, 7229-7246, 10.1002/2015jd023250, 2015.

Jin, X., Fiore, A., Boersma, K. F., Smedt, I., and Valin, L.: Inferring Changes in Summertime Surface Ozone-NO(x)-VOC Chemistry over U.S. Urban Areas from Two Decades of Satellite and Ground-Based Observations, Environ Sci Technol, 54, 6518-6529, 10.1021/acs.est.9b07785, 2020.

Jin, X., Fiore, A. M., Murray, L. T., Valin, L. C., Lamsal, L. N., Duncan, B., Boersma, K. F., De Smedt, I., Abad, G. G., Chance, K., and Tonnesen, G. S.: Evaluating a Space-Based Indicator of Surface Ozone-NO (x) -VOC Sensitivity Over Midlatitude Source Regions and Application to Decadal Trends, J Geophys Res Atmos, 122, 10-461, 10.1002/2017JD026720, 2017.

Kendall, M. G.: Rank Correlation Methods, 4th edn., Charles Grif- fin, London1975.

Krotkov, N. A., McLinden, C. A., Li, C., Lamsal, L. N., Celarier, E. A., Marchenko, S. V., Swartz, W. H., Bucsela, E. J., Joiner, J., Duncan, B. N., Boersma, K. F., Veefkind, J. P., Levelt, P. F., Fioletov, V. E., Dickerson, R. R., He, H., Lu, Z., and Streets, D. G.: Aura OMI observations of regional SO₂ and NO₂ pollution changes from 2005 to 2015, Atmospheric Chemistry and Physics, 16, 4605-4629, 10.5194/acp-16-4605-2016, 2016.

Kuttippurath, J., Abbhishek, K., Gopikrishnan, G. S., and Pathak, M.: Investigation of long–term trends and major sources of atmospheric HCHO over India, Environmental Challenges, 7, 10.1016/j.envc.2022.100477, 2022.

Li, K., Jacob, D., Liao, H., Shen, L., Zhang, Q., Bates., K. Anthropogenic drivers of 2013–2017 trends in summer surface ozone in China. Proceedings of the National Academy of Sciences 116, 422–427, 10.1073/pnas.1812168116, 2019

Liu, F., Beirle, S., Zhang, Q., Dörner, S., He, K., and Wagner, T.: NOx lifetimes and emissions of cities and power plants in polluted background estimated by satellite observations, Atmospheric Chemistry and Physics, 16, 5283-5298, 10.5194/acp-16-5283-2016, 2016.

LIU, R., ZHONG, M., ZHAO, X., LU, S., TIAN, J., LI, Y., HOU, M., LIANG, X., HUANG, H., FAN, L., and YE, D.: Characteristics of Industrial Volatile Organic Compounds(VOCs) Emission in China from 2011 to 2019, Environmental Science, 42, 5169-5179, 2021.

Lu, X., Hong, J., Zhang, L., Cooper, O., Schultz, M.: Severe Surface Ozone Pollution in China: A Global Perspective. Environ Sci Tech Let, 5, 487–494, 10.1021/acs.estlett.8b00366, 2018.

Malley, C. S., Henze, D. K., Kuylenstierna, J. C. I., Vallack, H. W., Davila, Y., Anenberg, S. C., Turner, M. C., and Ashmore, M. R.: Updated Global Estimates of Respiratory Mortality in Adults ≥30 Years of Age Attributable to Long-Term Ozone Exposure, Environ Health Perspect, 125, 087021, 10.1289/EHP1390, 2017.

Manisalidis, I., Stavropoulou, E., Stavropoulos, A., and Bezirtzoglou, E.: Environmental and Health Impacts of Air Pollution: A Review, Front Public Health, 8, 14, 10.3389/fpubh.2020.00014, 2020.

https://doi.org/10.5194/egusphere-2025-368
Preprint. Discussion started: 4 February 2025

Mann., H. B.: Nonparametric Tests Against Trend, Econometrica, 13, 245–259, 10.2307/1907187 1945.

Martin, R. V., Fiore, A. M., and Van Donkelaar, A.: Space-based diagnosis of surface ozone sensitivity to anthropogenic emissions, Geophysical Research Letters, 31, 10.1029/2004gl019416, 2004.

Martins, E. M., Nunes, A. C. L., and Corrêa, S. M.: Understanding Ozone Concentrations During Weekdays and Weekends in the Urban Area of the City of Rio de Janeiro, Journal of the Brazilian Chemical Society, 26, 1967-1975, 10.5935/0103-5053.20150175, 2015.

Mills, G., Harmens, H., Wagg, S., Sharps, K., Hayes, F., Fowler, D., Sutton, M., and Davies, B.: Ozone impacts on vegetation in a nitrogen enriched and changing climate, Environ Pollut, 208, 898-908, 10.1016/j.envpol.2015.09.038, 2016.

Monks, P. S., Archibald, A. T., Colette, A., Cooper, O., Coyle, M., Derwent, R., Fowler, D., Granier, C., Law, K. S., Mills, G. E., Stevenson, D. S., Tarasova, O., Thouret, V., von Schneidemesser, E., Sommariva, R., Wild, O., and Williams, M. L.: Tropospheric ozone and its precursors from the urban to the global scale from air quality to short-lived climate forcer, Atmospheric Chemistry and Physics, 15, 8889-8973, 10.5194/acp-15-8889-2015, 2015.

Nuvolone, D., Petri, D., and Voller, F.: The effects of ozone on human health, Environ Sci Pollut Res Int, 25, 8074-8088, 10.1007/s11356-017-9239-3, 2018.

Palmer, P. I., Jacob, D. J., Fiore, A. M., Martin, R. V., Chance, K., and Kurosu, T. P.: Mapping isoprene emissions over North America using formaldehyde column observations from space, Journal of Geophysical Research: Atmospheres, 108, 10.1029/2002jd002153, 2003.

Paoletti, E., De Marco, A., Beddows, D. C., Harrison, R. M., and Manning, W. J.: Ozone levels in European and USA cities are increasing more than at rural sites, while peak values are decreasing, Environ Pollut, 192, 295-299, 10.1016/j.envpol.2014.04.040, 2014.

Pfister, G. G., Walters, S., Lamarque, J. F., Fast, J., Barth, M. C., Wong, J., Done, J., Holland, G., and Bruyère, C. L.: Projections of future summertime ozone over the U.S, Journal of Geophysical Research: Atmospheres, 119, 5559-5582, 10.1002/2013jd020932, 2014.

Pierce, T., Hogrefe, C., Trivikrama Rao, S., Porter, P. S., and Ku, J.-Y.: Dynamic evaluation of a regional air quality model: Assessing the emissions-induced weekly ozone cycle, Atmospheric Environment, 44, 3583-3596, 10.1016/j.atmosenv.2010.05.046, 2010.

Raj, B. and Koerts, J.: Henri Theil's Contributions to Economics and Econometrics, Advanced Studies in Theoretical and Applied Econometrics, Springer Dordrecht, 345–381 pp., 10.1007/978- 94-011-2546-8_20, 1992.

Russell, A. R., Valin, L. C., and Cohen, R. C.: Trends in OMI NO_2 observations over the United States: effects of emission control technology and the economic recession, Atmospheric Chemistry and Physics, 12, 12197-12209, 10.5194/acp-12-12197-2012, 2012.

Schroeder, J. R., Crawford, J. H., Fried, A., Walega, J., Weinheimer, A., Wisthaler, A., Müller, M., Mikoviny, T., Chen, G., Shook, M., Blake, D. R., and Tonnesen, G. S.: New insights into the column CH2O/NO_2 ratio as an indicator of near-surface ozone sensitivity, Journal of Geophysical Research: Atmospheres, 122, 8885-8907, 10.1002/2017jd026781, 2017.

Schultz, M. G., Schröder, S., Lyapina, O., Cooper, O. R., Galbally, I., Petropavlovskikh, I., von Schneidemesser, E., Tanimoto, H., Elshorbany, Y., Naja, M., Seguel, R. J., Dauert, U., Eckhardt, P., Feigenspan, S., Fiebig, M., Hjellbrekke,

https://doi.org/10.5194/egusphere-2025-368
Preprint. Discussion started: 4 February 2025

A.-G., Hong, Y.-D., Kjeld, P. C., Koide, H., Lear, G., Tarasick, D., Ueno, M., Wallasch, M., Baumgardner, D., Chuang, M.-T., Gillett, R., Lee, M., Molloy, S., Moolla, R., Wang, T., Sharps, K., Adame, J. A., Ancellet, G., Apadula, F., Artaxo, P., Barlasina, M. E., Bogucka, M., Bonasoni, P., Chang, L., Colomb, A., Cuevas-Agulló, E., Cupeiro, M., Degorska, A., Ding, A., Fröhlich, M., Frolova, M., Gadhavi, H., Gheusi, F., Gilge, S., Gonzalez, M. Y., Gros, V., Hamad, S. H., Helmig, D., Henriques, D., Hermansen, O., Holla, R., Hueber, J., Im, U., Jaffe, D. A., Komala, N., Kubistin, D., Lam, K.-S., Laurila, T., Lee, H., Levy, I., Mazzoleni, C., Mazzoleni, L. R., McClure-Begley, A., Mohamad, M., Murovec, M., Navarro-Comas, M., Nicodim, F., Parrish, D., Read, K. A., Reid, N., Ries, L., Saxena, P., Schwab, J. J., Scorgie, Y., Senik, I., Simmonds, P., Sinha, V., Skorokhod, A. I., Spain, G., Spangl, W., Spoor, R., Springston, S. R., Steer, K., Steinbacher, M., Suharguniyawan, E., Torre, P., Trickl, T., Weili, L., Weller, R., Xiaobin, X., Xue, L., Zhiqiang, M., Chang, M. E., and Lewis, A.: Tropospheric Ozone Assessment Report: Database and metrics data of global surface ozone observations, Elementa: Science of the Anthropocene, 5, 10.1525/elementa.244, 2017.

Seguel, R. J., Morales, S. R., and Leiva, G. M.: Ozone weekend effect in Santiago, Chile, Environ Pollut, 162, 72-79, 10.1016/j.envpol.2011.10.019, 2012.

Sen, P. K.: Estimates of the Regression Coefficient Based on Kendall's Tau, Journal of the American Statistical Association, 63, 1379-1389, 10.1080/01621459.1968.10480934, 1968.

Sicard, P., Paoletti, E., Agathokleous, E., Araminiene, V., Proietti, C., Coulibaly, F., and De Marco, A.: Ozone weekend effect in cities: Deep insights for urban air pollution control, Environ Res, 191, 110193, 10.1016/j.envres.2020.110193, 2020.

Sillman, S.: The use of NOy, H2O2, and HNO_3 as indicators for ozone-NOx-hydrocarbon sensitivity in urban locations, Journal of Geophysical Research: Atmospheres, 100, 14175-14188, 10.1029/94jd02953, 1995.

Sillman, S.: The relation between ozone, NOx and hydrocarbons in urban and polluted rural environments, Atmospheric Environment, 33, 1821-1845, 10.1016/s1352-2310(98)00345-8, 1999.

Simon, H., Wells, B., Baker, K. R., and Hubbell, B.: Assessing Temporal and Spatial Patterns of Observed and Predicted Ozone in Multiple Urban Areas, Environ Health Perspect, 124, 1443-1452, 10.1289/EHP190, 2016.

Simon, H., Hogrefe, C., Whitehill, A., Foley, K. M., Liljegren, J., Possiel, N., Wells, B., Henderson, B. H., Valin, L. C., Tonnesen, G., Appel, K. W., and Koplitz, S.: Revisiting day-of-week ozone patterns in an era of evolving US air quality, Atmospheric Chemistry and Physics, 24, 1855-1871, 10.5194/acp-24-1855-2024, 2024.

Solberg, S., Bergström, R., Langner, J., Laurila, T., and Lindskog, A.: Changes in Nordic surface ozone episodes due to European emission reductions in the 1990s, Atmospheric Environment, 39, 179-192, 10.1016/j.atmosenv.2004.08.049, 2005.

Souri, A. H., Choi, Y., Jeon, W., Woo, J. H., Zhang, Q., and Kurokawa, J. i.: Remote sensing evidence of decadal changes in major tropospheric ozone precursors over East Asia, Journal of Geophysical Research: Atmospheres, 122, 2474-2492, 10.1002/2016jd025663, 2017.

Souri, A. H., Nowlan, C. R., Wolfe, G. M., Lamsal, L. N., Chan Miller, C. E., Abad, G. G., Janz, S. J., Fried, A., Blake, D. R., Weinheimer, A. J., Diskin, G. S., Liu, X., and Chance, K.: Revisiting the effectiveness of HCHO/NO_2 ratios for inferring ozone sensitivity to its precursors using high resolution airborne remote sensing observations in a high ozone episode during the KORUS-AQ campaign, Atmospheric Environment, 224, 10.1016/j.atmosenv.2020.117341, 2020.

https://doi.org/10.5194/egusphere-2025-368
Preprint. Discussion started: 4 February 2025

Stephens, S., Madronich, S., Wu, F., Olson, J. B., Ramos, R., Retama, A., and Muñoz, R.: Weekly patterns of Me´xico City's surface concentrations of CO, NO , PM and O during 1986–2007, Atmos. Chem. Phys., 8, 5313–5325, 10.5194/acp-8-5313-2008, 2008.

Sun, W., Shao, M., Granier, C., Liu, Y., Ye, C. S., and Zheng, J. Y.: Long-Term Trends of Anthropogenic SO2, NOx, CO, and NMVOCs Emissions in China, Earth's Future, 6, 1112-1133, 10.1029/2018ef000822, 2018.

Tang, W. Y., Zhao, C. S., Geng, F. H., Peng, L., Zhou, G. Q., Gao, W., Xu, J. M., and Tie, X. X.: Study of ozone "weekend effect" in Shanghai. , Science in China Series D: Earth Sciences, 51, 1354–1360, 10.1007/s11430-008-0088-2, 2008.

Tonnesen, G. S. and Dennis, R. L.: Analysis of radical propagation efficiency to assess ozone sensitivity to hydrocarbons and NOx: 2. Long-lived species as indicators of ozone concentration sensitivity, Journal of Geophysical Research: Atmospheres, 105, 9227-9241, 10.1029/1999jd900372, 2000.

Toro, C., Foley, K., Simon, H., Henderson, B., Baker, K. R., Eyth, A., Timin, B., Appel, W., Luecken, D., Beardsley, M., Sonntag, D., Possiel, N., and Roberts, S.: Evaluation of 15 years of modeled atmospheric oxidized nitrogen compounds across the contiguous United States, Elementa (Wash D C), 9, 10.1525/elementa.2020.00158, 2021.

Tsai, Y. I.: Atmospheric visibility trends in an urban area in Taiwan 1961–2003, Atmospheric Environment, 39, 5555–5567, 10.1016/j.atmosenv.2005.06.012, 2005.

van der A, R. J., Mijling, B., Ding, J., Koukouli, M. E., Liu, F., Li, Q., Mao, H., and Theys, N.: Cleaning up the air: effectiveness of air quality policy for SO2 and NOx emissions in China, Atmospheric Chemistry and Physics, 17, 1775-1789, 10.5194/acp-17-1775-2017, 2017.

Wang, F., Qiu, X., Cao, J., Peng, L., Zhang, N., Yan, Y., and Li, R.: Policy-driven changes in the health risk of PM(2.5) and O(3) exposure in China during 2013-2018, Sci Total Environ, 757, 143775, 10.1016/j.scitotenv.2020.143775, 2021.

Wang, Y. H., Hu, B., Ji, D. S., Liu, Z. R., Tang, G. Q., Xin, J. Y., Zhang, H. X., Song, T., Wang, L. L., Gao, W. K., Wang, X. K., and Wang, Y. S.: Ozone weekend effects in the Beijing–Tianjin–Hebei metropolitan area, China, Atmos. Chem. Phys., 14, 2419–2429, 10.5194/acp-14-2419-2014, 2014.

WHO: Review of Evidence on Health Aspects of Air Pollution e REVIHAAP Project. , Technical Report. World Health Organization, Regional Office for Europe, Copenhagen, Denmark., 2013.

Williams, J. E., Boersma, K. F., Le Sager, P., and Verstraeten, W. W.: The high-resolution version of TM5-MP for optimized satellite retrievals: description and validation, Geoscientific Model Development, 10, 721-750, 10.5194/gmd-10-721-2017, 2017.

Yasuhiro, S., Mitsuyo, S., Norimichi, T., and Hiroshi, B.: Analyses of the Ozone Weekend Effect in Tokyo, Japan: Regime of Oxidant (O_3 + NO_2) Production, Aerosol and Air Quality Research, 161–168, 10.4209/aaqr.2011.07.0102, 2012.

Zhang, J. J., Wei, Y., and Fang, Z.: Ozone Pollution: A Major Health Hazard Worldwide, Front Immunol, 10, 2518, 10.3389/fimmu.2019.02518, 2019.

Zhao, B., Wang, S. X., Liu, H., Xu, J. Y., Fu, K., Klimont, Z., Hao, J. M., He, K. B., Cofala, J., and Amann, M.: NOx emissions in China: historical trends and future perspectives, Atmospheric Chemistry and Physics, 13, 9869-9897, 10.5194/acp-13-9869-2013, 2013.

https://doi.org/10.5194/egusphere-2025-368
Preprint. Discussion started: 4 February 2025

Zou, Y., Charlesworth, E., Yin, C. Q., Yan, X. L., Deng, X. J., and Li, F.: The weekday/weekend ozone differences induced by the emissions change T during summer and autumn in Guangzhou, China, Atmospheric Environment, 199, 114-126, 10.1016/j.atmosenv.2018.11.019, 2019.